Federation University ResearchOnline

https://researchonline.federation.edu.au

Copyright Notice

This is the published version of:

Exploring the Dynamic Voltage Signature of Renewable Rich Weak Power System

SAEED ALZAHRANI [1,2], **(Student Member, IEEE), RAKIBUZZAMAN SHAH** [3], **(Member, IEEE),**
AND NADARAJAH MITHULANANTHAN [1], **(Senior Member, IEEE)**
[1]School of Information Technology and Electrical Engineering, The University of Queensland, Brisbane, QLD 4072, Australia
[2]Electrical Engineering Department, Faculty of Engineering, Al-Baha University, Al Bahah 65779, Saudi Arabia
[3]School of Engineering, IT and Physical Sciences, Federation University Australia, Ballarat, VIC 3353, Australia

Corresponding author: Saeed Alzahrani (s.alzahrani@uq.edu.au)

ABSTRACT Large-scale renewable energy-based power plants are becoming attractive technically and economically for generation mix around the world. Nevertheless, network operation has significantly changed due to the rapid integration of renewable energy in supply side. The integration of more renewable resources, especially inverter-based generation, deteriorates power system resilience to disturbances and substantially affects stable operations. The dynamic voltage stability becomes one of the major concerns for the transmission system operators (TSOs) due to the limited capabilities of inverter-based resources (IBRs). A heavily loaded and stressed renewable rich grid is susceptible to fault-induced delayed voltage recovery. Hence, it is crucial to examine the system response upon disturbances, to understand the voltage signature, to determine the optimal location and sizing of grid-connected IBRs. Moreover, the IBRs fault contribution mechanism investigation is essential in adopting additional grid support devices, control coordination, and the selection of appropriate corrective control schemes. This article utilizes a comprehensive assessment framework to assess power systems' dynamic voltage signature with large-scale PV under different realistic operating conditions. Several indices quantifying load bus voltage recovery have been used to explore the system's steady-state, transient response, and voltage trajectories. The recovery indices help extricate the signature and influence of IBRs. The proposed framework's applicability is carried out on the New England IEEE - 39 bus test system using the DIgSILENT platform.

INDEX TERMS Correlation, dynamic signature, dynamic VAr, load dynamic, large-scale integration, PV, voltage recovery index, voltage stability.

NOMENCLATURE

Acronyms:

DER	Distributed energy resources
DVAr	Dynamic reactive power
DVS	Dynamic voltage support
FIDVR	Fault induced delayed voltage recovery
FRT	Fault ride-through
IBR	Inverter-based resource
IVSI	Improved voltage stability index
LSPV	Large-scale photovoltaic
PCC	Point of common coupling
PLL	Phase-locked loop
PV	Photovoltaic
SC	Short circuit

SCR	Short-circuit ratio
SG	Synchronous generator
STATCOM	Static synchronous compensator
STVS	Short term voltage stability
TSO	Transmission system operators
VC	Voltage control mode
VDI	Voltage deviation index
VRI	Voltage recovery index
VSF	Voltage stability factor
WECC	Western electricity coordinating council

Variables:

A	Total number of voltage samples
b_s	Static load susceptance
Dyn %	Dynamic load percentage
f_e	Electrical frequency
g_s	Static load conductance
H	Inertia constant

The associate editor coordinating the review of this manuscript and approving it for publication was N. Prabaharan.

i_d^*	Direct axis current
i_{dref}^*	Direct axis reference current
i_{lim}^*	Current limit
i_q^*	Quadrature axis current
i_{qref}^*	Quadrature axis reference current
kp	Active power sensitivity factor
kq	Reactive power sensitivity factor
L	Total number of voltage sub-intervals
M	Total number of voltage constraints
P	Active power
P_0	Load size
$p_1 \& q_1$	Percentages of active and reactive power in constant impedance load
$p_2 \& q_2$	Percentages of active and reactive power in constant current load
$p_3 \& q_3$	Percentages of active and reactive power in constant power load
Q	Reactive power
Q_C	Transmission line charging capacitance
Q_{SG}	Synchronous generator steady state VAr
$QS\text{-}Transt$	Synchronous generator sub-transient VAr
$QTranst$	Synchronous generator transient VAr
x_d	Rotor resistance
s	Motor slip
S_{cr}	Critical slip
S_0	Normal operating slip
t	Proportion of the dynamic load
T_a	Acceleration time constant
t_1	Time limit 1 of WECC violation criterion
t_2	Time limit 2 of WECC violation criterion
t_{c1}	Time at fault clearing instant
T_e	Electrical torque
t_f	End of transient observation time
T_m	Mechanical torque
v	Voltage violation criteria of WECC
V_1	Voltage limit 1 of WECC violation criterion
V_2	Voltage limit 2 of WECC violation criterion
V_3	Voltage limit 3 of WECC violation criterion
V_{max}	Post disturbance maximum voltage
V_{min}	Post disturbance minimum voltage
V_0	Rated voltage
V_{pre}	Pre-fault steady-state voltage
vt	Voltage curve during the transient time
ω_r	Angular speed
X_d	Synchronous reactance
x_d	Rotor reactance
$X_{d'}$	Transient reactance
$X_{d''}$	Sub-transient reactance
X_l	Stator parameters
z_d	Induction motor equivalent impedance

I. INTRODUCTION

Photovoltaic and wind are the most widely used renewable energy resources due to resource availability, advancement in power electronics, and economic viability over other renewables. Moreover, the LSPV is at the forefront of the renewable energy market. A few GW size PV power plants are being built globally [1], [2]. Such a transformation in the energy sector would result in clean, green, and affordable energy. Nevertheless, the replacement of traditional SGs with the IBRs could lead to power system operation issues related to power quality, stability, and security of the power system [3], [4].

Fundamentally, IBRs are different from SGs. Therefore, the large integration of IBRs may deteriorate the stability of the system. The control strategy plays a vital role in the IBRs performance. The IBR controls are usually fast-acting to most of the system disturbances. Such features could introduce significant impacts on the system performances if the IBR controller was not well developed. A PLL is used to synchronize the IBRs to the grid. Consequently, the PLL is one of the main elements that defined IBR's dynamic response and performance under disturbances. Therefore, some oscillatory issues can be seen when IBR is integrated into weak bus and areas. Therefore, IBRs could jeopardize the system stability. Moreover, IBRs have limited fault current contribution (about 1.5 p.u.) in comparison to SGs (which can inject fault current up to 6 p.u. of its related current [5]). However, with an effective control scheme, IBRs could become more capable of complying with grid requirements or at least providing similar contributions that SGs used to provide in terms of voltage regulation and dynamic reactive power support. Several research efforts [6]–[9] have been made to explore the dynamic capability of IBRs in complying with the grid requirements. The research effort in [6] reviewed the LSPV power plant's connection requirements and highlighted the challenging issues related to system stability. The authors of [8] analyzed the FRT standard of large-scale IBRs. The DVAr support of the IBR attaining more attention recently. Several research works have been carried out to relate the LSPV system with the overall DVAr of the network. Research efforts in [10]–[12] have analyzed optimal reserve and location of DVAr resources to enhance the dynamic voltage stability of the grid, which is also known as short-term voltage stability.

STVS is one of the keys issues for a stressed grid due to the limited capability of IBRs. The STVS may occur after a large disturbance with insufficient dynamic VAr being injected into the grid. Power system with high pentation of induction motors is more vulnerable to STVS, especially in a renewable energy-rich grid. In such a condition, STVS is a consequence of FIDVR caused by decelerating and stalling of induction motors. Several research efforts had been made to investigate the FIDVR and proposed mitigation solutions. Paramasivam *et al.* [13] have developed an approach to optimally size and locate the dynamic reactive resources to avoid short-term voltage instability. The research work in [14] was devoted to investigates the impact of LSPV power plant control strategies on grid voltage stability. Moreover, an index called voltage recovery index was proposed to measure system post-disturbance response. The work developed

by Varma and Mohan in [15] proposed a novel day and night control scheme of LSPV called PV-STATCOM, which could mitigate FIDVR. The PV- STATCOM shows the effectiveness in improving STVS even though loads (induction motor) are located far away from the PV power plant. A stability margin has been proposed in [16] to help in understanding and analyzing the STVS. The influence of PV dynamics on the grid STVS is explored in [17]. Some countermeasures related to PV inverter operating conditions and DVS capability are also examined and found suitable to enhance grid voltage stability. Furthermore, an improved DVS capability was proposed in [17] by coordinating the injection of active and reactive power of PV inverter as a function of the inverter terminal voltage.

The aforementioned studies have examined the PV effect on the STVS with several novel methods for voltage and reactive power control proposed. Nevertheless, none of these studies has explored the impact of LSPV with verities of system prompters related to dynamic load percentages, PV penetration levels, and fault locations and the correlation of such with PV system operation and control. This research effort is aim to explore the dynamic voltage signature and influence of LSPV power plant on system transient response.

In this research, the influence of LSPV power plant on system steady-state and transient performance are thoroughly examined on a large multi-machine interconnected power system. The examination aims to extract and demonstrate the system dynamic voltage signature of a renewable rich power system. Several system aspects, which were overlooked in previous studies, have been comprehensively considered to figure out the system post-disturbance voltage recovery signature. These aspects include PV penetration level, load size, load dynamic percentage, bus SC level, and fault location. This research contributes towards a better understanding of system dynamic voltage signature under different realistic operating conditions by proposing an assessment framework considering both steady-state and transient analyses. The main contributions of this article can be summarized as follow:

- Explore the influence of LSPV power plants on system transient response from the viewpoint of dynamic voltage stability under various operating conditions.
- Propose a framework based on serval indices with complementary characteristics to assess the LSPV integration influence under a wide range of PV penetration levels and load dynamics.
- Investigate the relation between short circuit level and post-disturbance performance in the presence of IBRs.
- Determine and figure out the reason behind the system's dynamic trend of voltage recovery enhancement with more IBRs.

The simulation results clearly demonstrate the mechanism of the LSPV influence on system response upon disturbance. Considering PV's influence on system dynamic voltage signature, several aspects can be improved during planning and operation stages with the help of the proposed framework.

The rest of the paper is organized as follows. The test system and modeling overview of various components, including the LSPV plant, are described in Section II. Research methodology and assessment indices are presented in Section III. The steady-state and dynamic assessment results and discussions are given in Section IV. The paper is concluded in Section V.

II. MODELLING OVERVIEW
A. TEST POWER SYSTEM
The 10-machines (60Hz) 39 bus New-England power system, widely known as the IEEE 39 bus system, is used here as the test system [18]. A modification has been made to observe the impact of LSPV power plants on the dynamic reactive power capability of a stressed or weak grid. Generally, the lesser amount of the fault current, the smaller the short circuit ratio. Therefore, the weaker the grid, the less stable system [19]. The IEEE 39 bus system can be divided into three zones, as given in Fig. 1. Each zone has its own characteristics in terms of SC MVA level. For example, Zone 1 has the lowest average SC level for load buses. On the other hand, Zone 3 has the highest SC level. Other zonal characteristics and their responses to system disturbances are explored in detail in the assessment section. The system has several SGs, as indicated in Fig. 1.
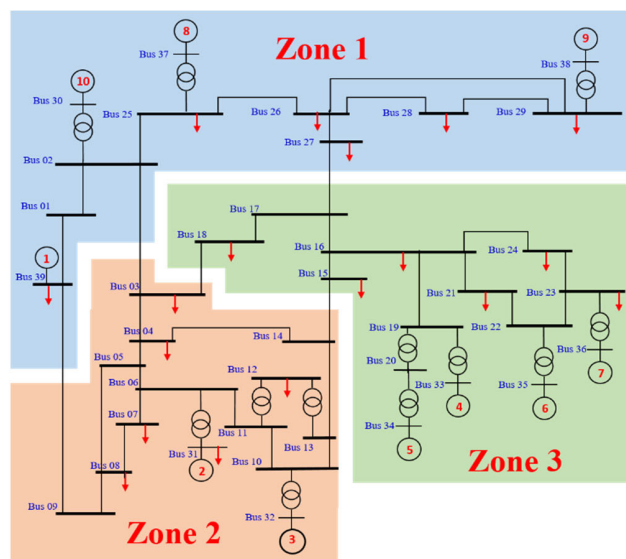

FIGURE 1. IEEE 39 Bus test system [18].

B. GENERATOR MODEL
In IEEE 39 bus test system, there are ten machines. The SG 1 represents the connection of the test system, i.e., the New England network to the rest of the North American grid. Therefore, the detailed dynamic model of this machine was not considered as it is representing a very large system. The rest of the SGs are modeled in detail with their sub-transient and transient reactances, which are given in Table 1. Generators SG 2 - 10 are equipped with IEEE Type 1 automatic

TABLE 1. Synchronous generator parameters [20].

SG	MVA	H (s)	X_L (p.u.)	X_D (p.u.)	$X_{D'}$ (p.u.)	$X_{D''}$ (p.u.)
2	700	4.33	0.25	2.07	0.49	0.35
3	800	4.47	0.24	2.00	0.43	0.36
4	800	3.57	0.24	2.10	0.35	0.28
5	300	4.33	0.16	2.01	0.40	0.27
6	800	4.35	0.18	2.03	0.40	0.32
7	700	3.77	0.23	2.07	0.34	0.31
8	700	3.47	0.20	2.03	0.40	0.32
9	1000	3.45	0.30	2.11	0.57	0.45
10	1000	4.20	0.13	1.00	0.31	0.25

voltage regulator. The speed governor is also installed in SG 2 - 10. Steam turbine governor class IEEE Type G1 is used for SG 2 - 9. Generator SG 10 is equipped with hydro turbine governor class IEEE Type G3. The transmission lines of the system are modeled with the standard π equivalent circuit. The MVA rating is not only sufficient to equate SGs capabilities. Nevertheless, other parameters are introduced to identify the constraints on the dynamic performances of SG. For example, SG 9 is rated at 1000 MVA; however, transient reactance is almost double of SG 10. Therefore, it is expected that the SG 10 may have better dynamic performance and contribution than the SG 9. Based on that, some SGs could be classified as weak SG. Later, the influence of retiring such a generator and replacing them with IBRs is explored. The model of other power sources, i.e., LSPV is mentioned in the following section.

C. LSPV MODEL

In this research, and due to the unavailability of real LSPV power plant data, a WECC LSPV plant model with the Electrical Control Model (REEC_B) and the Generator-Converter Model (REGC_A) is used [21]. Based on the grid code, the LSPV system should support system voltage by injecting or absorbing reactive power at PCC [5], [22], [23]. This can be achieved by operating the PV inverters in voltage or reactive power control modes [24]. Other approaches that can be used such as the installation of STATCOM or synchronous condenser at the PCC with unity power factor operation of PV system [25]. However, more investigations are still required to identify the economic feasibility of using STATCOM and synchronous condenser at the PV terminal.
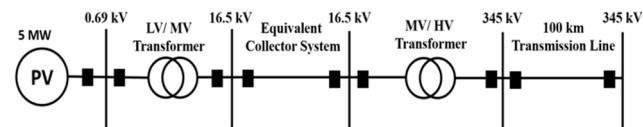

FIGURE 2. PV system layout.

Fig. 2 demonstrates the PV system layout. The PV inverter converts the DC power to a low voltage (LV) AC power at 0.69 kV. Then, a 5 MVA medium voltage (MV) transformer is used to step up the voltage to 16.5 kV. Several PV units are connected through MV feeders to the main MV bus.

The accumulative plant power is then directed through an MV/HV transformer to 345 kV. Hence, LSPV power plants are usually erected far from the load center. Therefore, a 100 km transmission line is considered here between the PV plant and PCC.

In this investigation, the VC of the PV inverters is used to mimic the operational features similar to SG. The plant controller works to attain the PCC set voltage. This can be achieved by assigning the required VAr among the PV inverters. Different d and q axis current limits can be applied to the converter based generator. A fixed d and q current limit have been used. In this current limit, the concept comprises of fixed current limit. This means that the converter system remains connected to the system without injecting any additional reactive current. This is a widely used current limit logic in literature. Three different current priorities can be used for such current limit logic. These can be stated as -

1) Active and reactive current have equal priority.
2) Active current has higher priority than reactive current.
3) Reactive current has higher priority than active current.

While designing the fixed current limiter in this article, the active current is prioritized in the outputs of the current magnitude. The fixed current limit with active current priority can be defined by (1) & (2). Power system loads affect the grid ability to respond to system disturbance. Therefore, load modeling is presented in the next section, as it is a critical aspect of dynamic voltage stability studies.

$$i_d^* = max\left(i_{lim}^*, i_{dref}^*\right) \qquad (1)$$

$$i_q^* = max(\sqrt{i_{lim}^{*2} - i_q^{*2}}, i_{qref}^*) \qquad (2)$$

D. LOAD MODEL

There are a variety of loads in power systems such as residential, commercial, and industrial loads. Those loads have different responses during the steady-state and transient timeframe [26]. Therefore, it is important to include the load characteristics in power system studies. It is impractical to represent the actual loads at each load bus due to the uncertainty associated with load characteristics, time of operation, and complexity associated with such representation. Therefore, the modeling of the load with an acceptable degree of accuracy is the common practice in power utilities. Typically, power system loads are modeled as exponential, polynomial, or composite loads [26], [27]. In the exponential model, the active and reactive power of the load at a specific voltage can be found as a function of the power drawn at the rated voltage, as expressed in (3) & (4) [28].

$$P = P_0(\frac{V}{V_0})^{k_p}, 0 \leq k_p \leq 4 \qquad (3)$$

$$Q = Q_0(\frac{V}{V_0})^{k_q}, 0 \leq k_q \leq 8 \qquad (4)$$

The second model is the polynomial load, which is also known as ZIP model. In the ZIP model, the load is made up of the constant impedance (Z), current (I), and power (P)

at different percentages determined by *p1, p2 & p3,* and *q1, q2 & q3.* The active and reactive power of ZIP load can be expressed as in (5) & (6) [27].

$$P = P_0[p1(\frac{V}{V_0})^2 + p2(\frac{V}{V_0}) + p3], \sum_{i=1}^{i=3}(p_i) = 1 \quad (5)$$

$$Q = Q_0[q1(\frac{V}{V_0})^2 + q2(\frac{V}{V_0}) + q3], \sum_{i=1}^{i=3}(q_i) = 1 \quad (6)$$

The third model is the composite load model which is commonly used model for dynamic stability studies [26]. The composite model combines the static and dynamic loads to precisely represent the relationship between the load's active and reactive power and the bus voltage. Different approaches have been used to model the load for dynamic studies. However, the use of a polynomial load model (ZIP load) in parallel to an induction motor, as depicted in Fig. 3, is the general practice in the North American utilities [26] for dynamic studies. The currents drawn by the static and dynamic parts of the composite load are represented by (7) - (13). The precise representation of the composite load parameters may influence the accuracy of the stability studies. Nevertheless, according to the research effort reported in [29], the most influential parameters for the transient stability studies are the size of the load, the normal operating slip, critical slip, the proportion of the dynamic load, and the acceleration time constant.
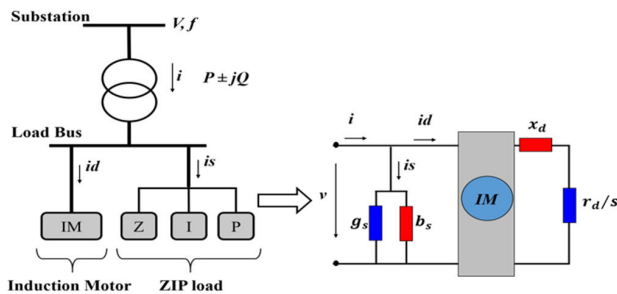

FIGURE 3. Composite load model.

The conductance and susceptance of the static load as given in Fig. 3 can be expressed by (9) & (10). The dynamic part of the composite load is modeled as a simplified induction motor. The equivalent impedance of the motor can be found from the respective rotor resistance and reactance. The slip of the induction motor can be found from the relationship between f_e and ω_r as in (12) & (13).

$$i = i_s + i_d \quad (7)$$

$$i_s = v(g_s\frac{p}{p_0} + jb_s\frac{q}{q_0})\frac{v_0^2}{v^2} \quad (8)$$

$$g_s = \frac{p_0}{v_0^2}(1 + t_{m0}) \quad (9)$$

$$b_s = -\frac{q_0 - p_0 t_{m0}(S_0/S_{cr})}{v_0^2} \quad (10)$$

$$i_d = \frac{v}{z_d} = \frac{v}{(r_d/S_0) + jx_d} \quad (11)$$

$$s = f_e - \frac{\omega_r}{2\pi} \quad (12)$$

$$\frac{d\omega_r}{dt} = \frac{T_e - T_m}{T_a} \quad (13)$$

In this work, values suggested by various TSOs are considered for the composite load modeling. These values presented in Table 2 have resulted from a case study as reported in [28].

TABLE 2. Composite load parameters [28].

Parameters	p_1	p_2	p_3	q_1	q_2	q_3	S_0	S_{cr}	T_a (S)
Value	0.552	0.338	0.110	0.599	-1.427	1.828	1.35	10.29	0.93

III. METHODOLOGY

In a complex power system, it is of great interest to explore the dynamic voltage signature and the influence of each component on the system. Therefore, an appropriate mitigation technique can be applied effectively at the right time and suitable locations. The current power system is usually operated under stressful conditions with uncertainty both in the generation and demand. The transient responses of load buses are influenced by several factors such as load size, loading condition, dynamic load percentages, and the availability of the DVAr. The steady-state analysis is performed to figure out the SGs VAr reserve and the VAr flow on the network. The SC calculations are performed as well to calculate the load buses SC MVA level. The dynamic response is initially assessed for the base case scenario under different dynamic load percentages without IBRs. Later, the influence of IBR penetrations is assessed for similar dynamic load levels. The impact of different loading conditions on the system transient response is also investigated at different PV pentation levels.

In this work, the transient system response is examined under the most severe disturbance and fault condition i.e. a three-phase solid SC at load buses. The faults are cleared after 100 ms, and the transient voltage profiles (approximately four seconds after the faults) are used to evaluate the network performance. The time-domain simulations are performed by DIgSILENT PowerFactory, a commercial-grade analytical software tool [20]. The influence of the dynamic composition of load on the system recovery is examined for 100% static load to 60 % dynamic load. The load bus voltage recovery is assessed to get an improved understanding of the performance of each load bus. Later, the system response is reviewed with IBRs with different percentages of load dynamics. Several indices are used to assess the post-fault response numerically to figure out the dynamic voltage signature and influence of IBRs on dynamic system responses.
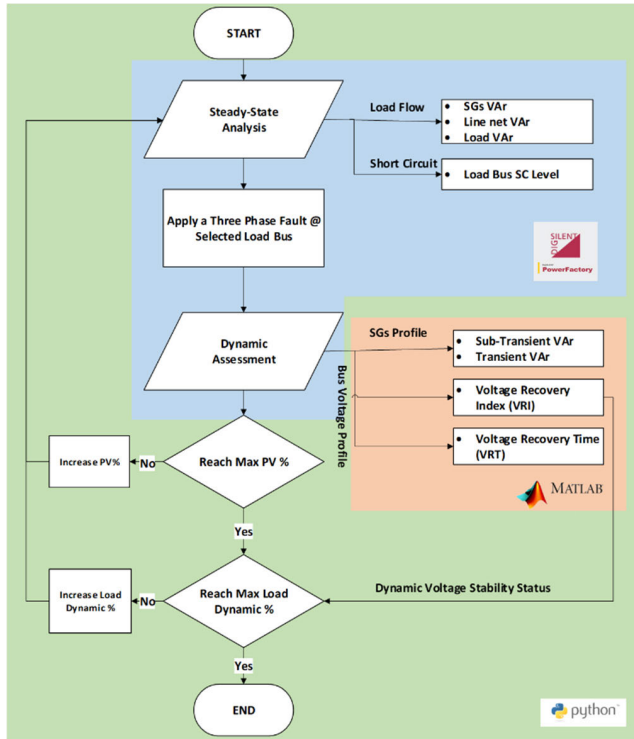
Fig. 4 illustrates the flowchart of the proposed assessment framework starting with the steady-state assessment that includes the power flow and SC calculations. Then, the dynamic assessment is carried out to explore the post fault response under different realistic operating conditions. Python programming is utilized to automate the time-domain simulation in which the PV penetration level and dynamic load percentages are increased in each simulation loop. MATLAB is used to calculate the post-fault performance indices. The outcome of the steady-state and dynamic assessments are used to extract the system dynamic voltage signature under different realistic operation scenarios.

A. ASSESSMENT INDICES

For a renewable rich network with high penetration of induction motor loads, a voltage recovery performance of the load bus is a crucial aspect towards voltage stability [14]. Serval indices can be used to evaluate the voltage recovery, such as VDI, IVSI, and VSF, and others [16]. In this research, the voltage recovery index VRI is used [14]. Moreover, the SGs area of influence is also applied to link the voltage recovery performance of each load bus with the dynamic VAr capability of each SG. Hence, the VRI reflects all transient periods. Other indices i.e. QS-Transt, QTranst, and VRT are also used to evaluate the recovery at a specific post fault time frame. The combination of these indices is useful in sizing the LSPV plant, justify the requirement of additional VAr, their optimal size, and location for other VAr resources as well as the optimal tuning of the coordinated control method of the LSPV and other VAR resources.
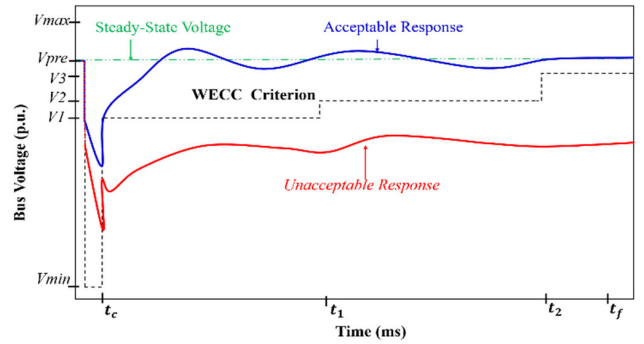
1) VOLTAGE RECOVERY INDEX (VRI)

Lammert [14] had investigated the fault-induced delayed voltage recovery, and VRI was proposed to examine the post fault performance. The VRI is a useful index that can be used to investigate the short-term voltage stability issue and other concerns related to the optimal control approaches of grid-connected IBRs. The VRI uses the WECC criterion as a reference to benchmark the transient voltage behavior of the load bus, as shown in Fig. 5. The VRI can result in a value between 1 and -1, where one means the bus voltage returns to its pre-fault level within the required time. On the other hand, -1 means the bus voltage does not recover at all. If VRI equals zero, it means the transient voltage of the load bus meets the minimum requirements of the grid code.

The following pseudocode briefly outlines the main steps in calculating the voltage recovery of the load bus [14]. The parameters used in the VRI calculation are given in the nomenclature.

Step 1: Define the voltage violation criteria, V_{WECC} was used as in (14).

Step 2: Partition the voltage between V_{max} and V_{min} into L sub-intervals (samples).

Step 3: Define the probability density function p^{VRI+} & p^{VRI-} of the voltage samples.

Step 4: Define and apply the weighting function to reward (η_j^+) or penalize (η_j^-) the voltage recovery.

Step 5: Calculate the VRI according to (15).

$$V_{WECC} = \begin{cases} V(t) \geq V_1 \text{ for } t_{c1} \leq t \leq t_1 \\ V(t) \geq V_2 \text{ for } t_1 \leq t \leq t_2 \ \& \text{ and } V_2 > V_1 \\ V(t) \geq V_3 \text{ for } t_2 \leq t \leq t_f \ \& \text{ and } V_3 > V_2 \end{cases} \quad (14)$$

$$VRI = \frac{1}{A} \sum_{j=1}^{M} \sum_{i=1}^{L} \left(\eta_{ji}^+ p_{ji}^{VRI+} + \eta_{ji}^- p_{ji}^{VRI-} \right) \quad (15)$$

2) SG AREA OF INFLUENCE

An area of influence of SG has been used to explain the effect of each SG on voltage recovery of each load bus. For a large and interconnected power system, not all the SGs would have the same influence on the voltage recovery of the load buses. Therefore, an idea of looking into the effect of SG outage on

the SC level of each load bus has been utilized to examine the impact of SG's DVAr capability on a load bus voltage recovery. The SC level at each load bus mainly depends on the rating of the SG and the electrical distance between the fault current source and the fault sink.

For a mesh network, when a fault occurs at any load bus, the SGs and other fault current sources would be aware of the fault incident in different degrees based on the electrical distance from the fault. Accordingly, different fault current contributions from generators would flow in a mesh network. In the base case (with all SGs), each bus has its specific SC level $Bus_{i\,old_{SC}}$ which would drop after an outage of SG_j to a new value $Bus_{i\,new_{SC}}$. Then, the percentage of change in the bus SC level is multiplied by $SG_j\_MVA_{norm}$ which represents the weighted MVA level of the SG_j. Therefore, the load bus SC sensitivity (Bus_iSCS_j) can be estimated by (16).

$$Bus_iSCS_j = SG_j\_MVA_{norm}(1 - \frac{Bus_{i_{newSC}}}{Bus_{i_{oldSC}}}) \qquad (16)$$

3) VOLTAGE RECOVERY TIME (VRT)
The VRI summarizes the transient response of the load bus over few seconds. Such an index is not sufficient to explore the PV impacton system dynamic response. It is essential to examine the bus performance during the first few cycles after the fault is cleared. After the post fault, the time required to reach the voltage to a certain level of pre-fault value referred to as voltage recovery time. The VRT highlights the system response in the transition stage from sub-transient to transient in which FIDVR commonly occurred. Focusing on the first few cycles after the fault clearance would identify the area of influence of PV integration. Moreover, the VRT may be used to propose a mitigation solution such as dynamic VAr support to improve system voltage recovery when IBRs are being integrated into the network.

4) DYNAMIC VAR SUPPORT (DVAR)
The reactive power output capability of SG can be classified into three regions. In the first region, the SG has an immediate response to the SC. This region can last for few cycles (milliseconds) and is known as the sub-transient region. The sub-transient reactance of SG influences the amount of fault current injection during the fault. The second region is known as the transient region which lasts for few seconds after the disturbance. The transient reactance of SG influences the SG response in this region. After few seconds of disturbance, the SG should return to its third region which refereed as the steady-state region. In this region, the SG VAr is influenced by the synchronous reactance of the generator [30].

The amount of reactive power injected from SGs and LSPVs during the disturbance (sub-transient and transient VAr) is estimated for each scenario. Exploring the nature of system recovery and dynamic VAr support under different operation conditions would help in understanding the degree of correlation between system parameters.

IV. RESULTS AND DISCUSSIONS
A. STEADY-STATE ASSESSMENT
The steady-state performance of the power system with LSPV power plants and the demand for reactive power has been carried out in this section. The reactive power flow map and the area of influence of SG are used for the assessment.

1) REACTIVE POWER FLOW MAP
System reactive power flow map including VAr capability of source and demand and VAr reserve are of high interest for voltage stability investigations and mitigation solutions. The reactive power of the IEEE 39 bus test system (Fig. 1) with its three zones is summarized in Fig. 6. Q_C and Q_{SG} are the main reactive power sources. The VAr is absorbed by the loads, line reactance, and transformers windings. The VAr reserve can be defined as the additional steady-state VAr that a generator can supply to a power system. In other words, VAr reserve is the result of subtracting SG injected VAr from SG maximum steady-state VAr capability.
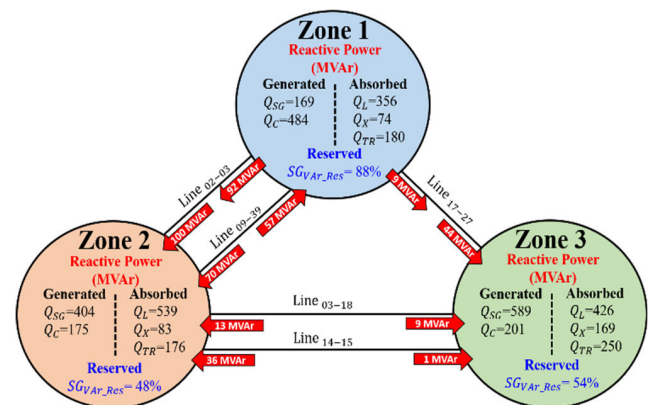

FIGURE 6. Reactive power flow in IEEE 39 bus system.

Each zone has distinct characteristics in terms of generation, absorption, and reserve of VAr. There is a reactive power flow between the zones according to the system operating conditions. In the base case, Zone 1 has a surplus VAr which is supplied to Zones 2 and 3. The VAr coming from the Q_C is very substantial at Zone 1 compare to Zone 2 & 3. Zone 1 has the highest reserve, followed by Zone 3 and 2, respectively.

2) SG AREA OF INFLUENCE
The area of influence of each generation unit on the load buses is used to identify the most dominant machine influencing the transient response of that bus. The percentage reduction on the load bus SC level with the outage of each ofSG units is presented in Table 3.

The dominant SG corresponding to each load bus can be selected based on the highest SC value. For example, the outage of SG 2 would reduce the SC level at bus 03 by 4%. On the other hand, if SG 10 is taken out of service, the SC level at bus 03 is reduced by 17%. Hence, SG10 outage represents the largest SC sensitivity to bus 03. Therefore, SG 10

TABLE 3. Area of influence (%) of the Sg.

Load Bus	Synchronous Generator								
	SG 02	SG 03	SG 04	SG 05	SG 06	SG 07	SG 08	SG 09	SG 10
3	4	5	2	1	3	2	6	4	17
4	9	11	3	1	3	2	3	3	8
7	12	11	2	2	2	2	3	3	5
8	12	11	2	2	2	2	3	3	5
15	3	5	5	2	6	4	2	3	4
16	2	3	9	4	10	6	2	4	5
18	3	3	3	2	4	3	4	5	11
21	1	2	4	2	15	8	1	2	2
23	1	1	2	1	18	18	1	1	1
24	2	2	6	3	9	7	2	3	4
25	2	2	1	1	1	1	17	7	22
26	1	1	1	1	2	1	6	22	9
27	1	2	2	1	3	2	4	13	7
28	0	0	0	0	0	0	2	37	3
29	0	0	0	0	0	0	2	48	3

is considered as the most influential machine on that bus. A similar SC sensitivity analysis can be carried for all other load buses and presented in Table III. It can be noticed that some load buses have very high sensitivity with respect to the outage of a particular machine such as Bus 29 to SG 9. Other machine outages may have a limited impact on bus 29. Besides, some load buses may be influenced by more than one machine such as bus 15, 16, 18, and 24. For simplicity, the most influential machine corresponding to each load bus with the highest sensitivity value is highlighted in Table 3.

B. DYNAMIC ASSESSMENT
By the steady-state assessment outcomes, the system response during the transient would be interpreted from the viewpoint of the VAr capability of SG, SG area of influence, *VRI*, and other assessment indices.

1) DYNAMIC ASSESSMENT COMPUTATIONAL COST
In this investigation, several scenarios representing realistic operating conditions are carried out in DELL computer by usingDIgSILENT PowerFactory 2019(X64) and Python 3.8. The computer has a processor of 3.6GHz Intel®core^{TM} i7-7700 CPU and 16.0 GB installed memory (RAM). In this assessment, the PV penetration level changed from 0% to 40%, with a 10% increment in each step. Load dynamic percentages changed from 0% to 60% with an increment step of 5%. The time-domain simulation is carried out for all system buses (i.e., 39 buses) with an integration step size of 1 ms. In each simulation loop, the disturbance is applied to the corresponding bus after 1s and cleared after 100 ms, and the transient response gets recorded for four seconds. The system buses voltage profile and SGs & PVs active and reactive power get recorded in each case. The simulation covered all the scenarios after three hours and eight minutes (03:08), and there are 2535 files (39*13*5) with a size of 6.4 GB.

2) TRANSIENT INFLUENCE OF LOAD DYNAMIC
In this section, the impact of increased load dynamics on the system voltage stability is studied for all the load buses.

This investigation aims to explore the dynamic load hosting capability of each load bus. Moreover, the outcome of this investigation can be used as a base case to explore the dynamic voltage stability signature with LSPV systems. The percentage of load dynamic negatively affects the transient response of the load bus. For a post fault voltage recovery, the need for the fault current is proportionally related to dynamic percentage of load.If there is an inadequate fault current supply to the fault location, the dynamic part of the load such as induction motors could stall. This may be followed by other local disturbance events which could eventually lead to global transient instability.
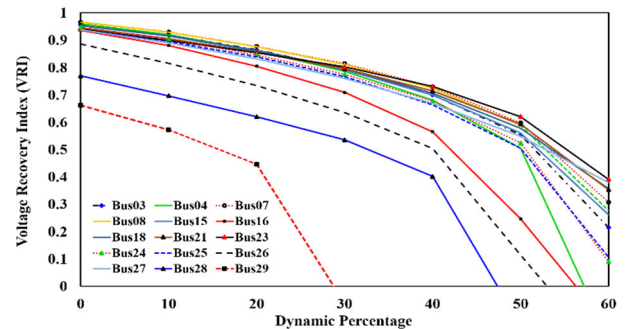

FIGURE 7. Impact of the dynamic load on system voltage recovery.

In this part, the percentage of the dynamic load is varied for all the load bus from 0 %, (i.e. static load) to 70% with step of 10%. For each dynamic load case, a three-phase SC fault is applied to the load bus separately and the VRI is calculated. Fig. 7 illustrates the load bus voltage recovery performance under different dynamic percentages of loads. In general, the trend is downward, this means that with the increase in dynamic load the voltage recovery performance is slowing down. Load buses can be categorized into three groups.

The first group is capable of hosting a high percentage (more than 60%) of a dynamic load. The second group can host about 50-60% dynamic load before those buses experienced voltage instability. The second group includes buses 16, 18, and 26. The third group includes load bus 28 and 29 has a lower capability in hosting more dynamic load. For instance, load at bus 29 suffers from a transient instability if dynamic load percentage is greater than 30%. Moreover, it can be observed as in Fig. 8 that the rate of change of the *VRI* with the increase of the dynamic load is not consistent for all the load buses, especially at the higher percentage of load dynamic. For example, bus 16 and 27 have the same VRI with a static load; however, bus 27 can host more than 60 % dynamic load compared to bus 16. It is worth noting that the higher dynamic load percentage at weak bus results in a delayed voltage recovery that leads to system transient instability. For instance, a fault at bus 29 (with 30% dynamic load) causes a delay in the voltage recovery that resulted in a rotor angle instability, as given in Fig. 8. Another example is the response of load at bus 16, where a delayed recovery
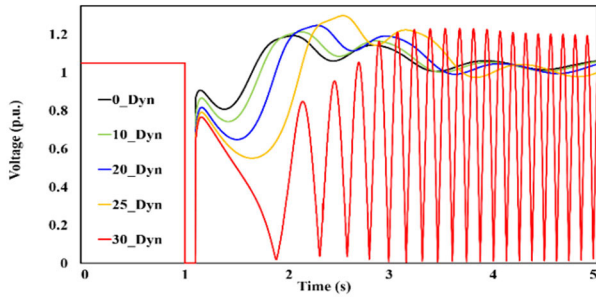
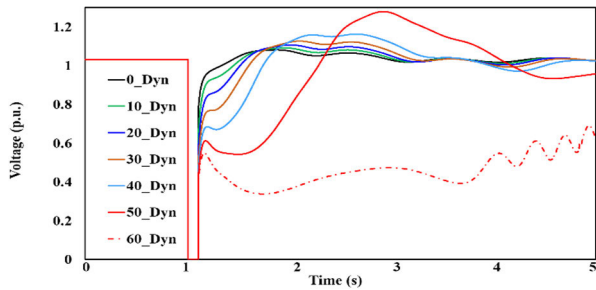**FIGURE 8.** Voltage under different dynamic load percentages – bus 29.

FIGURE 9. Voltage under different dynamic load percentages – bus 16.

can be seen with a 50% dynamic load. However, a voltage collapse would occur if the dynamic percentage of the load at bus 16 is about 60%, as given in Fig. 9.

TABLE 4. Load bus performance ranking.

Bus #	Load size MW	*SC* level MVA	VRI @ (0% Dyn)	*SC* ranking	VRI ranking
Bus 03	322	5344	0.956	2	4
Bus 04	500	4659	0.960	9	3
Bus 07	234	3673	0.966	13	1
Bus 08	522	3680	0.966	12	2
Bus 15	320	4910	0.953	6	6
Bus 16	329	6542	0.936	1	12
Bus 18	158	4986	0.954	5	5
Bus 21	274	4829	0.946	8	8
Bus 23	248	4906	0.940	7	9
Bus 24	309	5256	0.947	3	7
Bus 25	224	5244	0.938	4	10
Bus 26	139	4091	0.886	10	13
Bus 27	281	4069	0.938	11	11
Bus 28	206	2571	0.769	15	14
Bus 29	284	2921	0.662	14	15

The transient response of load bus represents the system characteristics which are influenced by several parameters in the network such as SC level, dynamic VAr, load types and size. Table 4 shows the load size, bus SC level, bus SC ranking, and Bus VRI ranking. From Table 4, it is clear that the bus SC level is not exceedingly correlated with the bus VRI (correlation coefficient R = 0.637). For example, bus 16 has the highest SC level, whereas its post fault transient response is ranked as 12th. On the other hand, bus 7 has the top VRI, while its SC level is the 3rd from the last. Table 5 shows the correlation coefficient between load buses' SC and VRI under

TABLE 5. Correlation coefficient between load buses' SC and VRI under different load dynamic percentages.

Correlation coefficient	Dyn %						
	0	10	20	30	40	50	60
R	0.637	0.625	0.601	0.533	0.518	0.512	0.220

different load dynamic percentages. The correlation coefficient is inversely related to the load dynamic percentage. From these results, it is not clear how different elements can affect the system strength and transient response. Therefore, a further investigation is required to identify the role and weight of the system's main elements influencing the voltage recovery of the load buses, especially with high penetrations of IBRs into the network. The additional investigation results are given in the subsequent sections.

3) PV INTEGRATION IMPACT
The exploration of the LSPV signature and impact on system transient response is carried out in this section. First, the impact of PV is assessed under different load dynamics percentages. By doing so, the system transient response can be figured out and be compared with the case without PV integration. Second, the response of the system is evaluated under a stressed situation with certain load dynamic percentages of each zone.
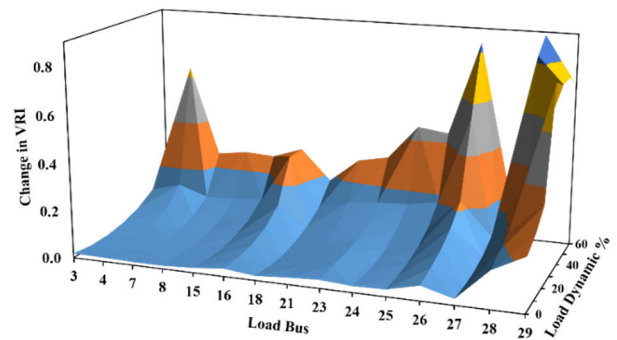

FIGURE 10. Load bus VRI improvement for the case of 40% PV.

a: UNDER DIFFERENT LOAD DYNAMIC
In this part, the MVA rating of SGs is reduced and an equivalent MVA of LSPV is integrated into the grid. Similar to the previous case, the impact of the dynamic load is explored under different PV pentation levels. From the simulation results, it is evident that the load bus transient response is improved when more PV being connected to the system. Fig. 10 demonstrates the changes in VRIs under different dynamic percentages when 40% of the SGs are replaced by LSPV power plants. It is evident that the PV is positively affecting the transient response of all load buses. The major influence of the PV system can be seen at higher dynamic load percentages. The loads at Zone 1 are benefited the most from PV integration, followed by loads at Zones 3 and 2.
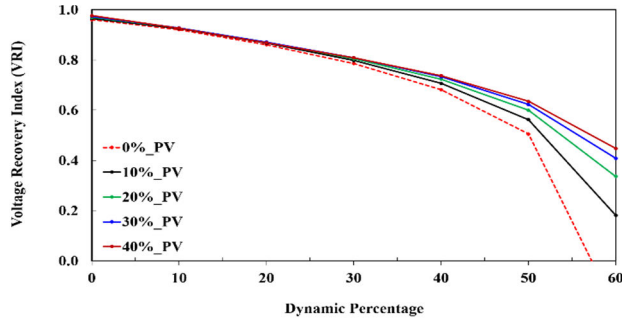
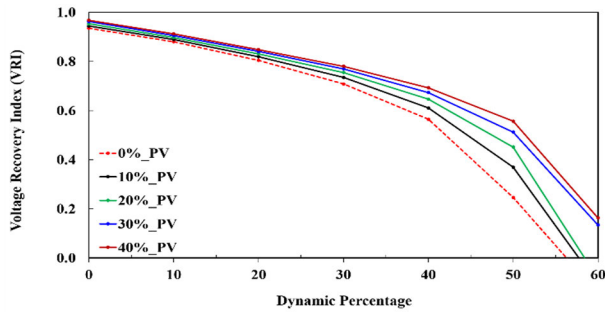**FIGURE 11.** VRI under different PV and load dynamic – bus 4.

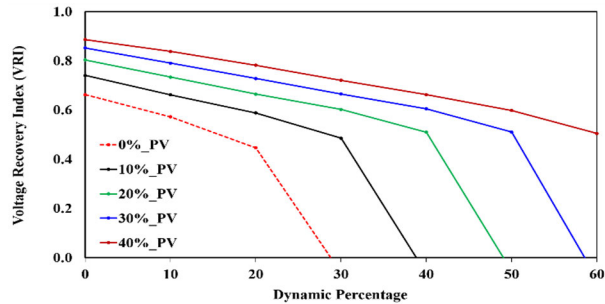**FIGURE 12.** VRI under different PV and load dynamic - bus 16.

FIGURE 13. VRI under different PV and load dynamic – bus 29.

The load buses 4, 16, and 29 (lowest VRI in each zone) are considered to highlight the response of each zone under different PVs and load dynamics, as shown in Figs. 11 - 13. The impact of PV on bus 4 is negligible at a lower percentage of dynamic loads in the system. However, the PV system enhanced the stability limit of bus 4. A similar trend can be seen on bus 16, where a slight improvement of VRI can be observed at a lower dynamic percentage of the load. Unlike buses 4 &16, bus 29 shows a significant improvement of its VRI when certain SG units are replaced by LSPV power plants. This improvement is significant even for the static load. The hosting capability for more dynamic load has substantially been improved from less than 30% (at the base case) to more than 60% with 40% PV. Even though the VRIs have been improved with PV, the signature of PV on the system transient response is yet to be determined. The next section highlights the PV signature during the disturbance.
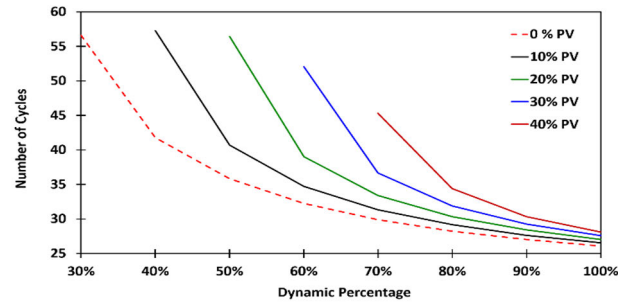

FIGURE 14. SG 9 out of step occurrence time after fault clearance.

It can be further noticed that PV integration can enhance the generator angular stability under some fault conditions similar to what has been found in the other research work [31], [32]. As can be seen from Fig. 8 that the bus 29 could have a delayed voltage recovery followed by a pole slip of SG 9. This may lead to angular instability. Fig. 14 demonstrates the SG 9 out of step time (in cycles) after the fault clearance and under different scenarios of dynamic load and PV penetration levels. The higher dynamic percentage may negatively affect the system transient stability by accelerating the SGs pole slip (out of step) time. On the other hand, more PV would enhance the grid voltage recovery as illustrated beforehand and delayed the SG's pole slip time. For instance, a pole slip happens at SG 9 after 32 cycles after fault clearance under 60% dynamic load for a three-phase fault occurs at bus 29. However, 30% PV improved the angler stability margin of SG 9 by delaying the pole slip time to 52 cycles after clearing the fault. Moreover, the impact of PV on the angular instability is significant at lower percentages of dynamic load. Nevertheless, at higher percentages of dynamic load PV impact on SGs out of step time is minimal.

TABLE 6. System VRI with maximum load dynamic at each zone.

Load Bus	3	4	7	8	15	16	18	21	23	24	25	26	27	28	29
Zone			2					3					1		
Dyn %			30					45					20		
VRI	0.8	0.8	0.8	0.8	0.8	0.6	0.8	0.8	0.8	0.7	0.8	0.6	0.8	0.6	0.2

b: UNDER FIXED LOAD DYNAMIC

It can be seen from the prior section that PV integration could improve the short term voltage stability of the system. However, the mechanism of the PV contribution on system transient response is not yet fully understood. PV contribution mechanism can be explored for a stressed network after assigning a certain dynamic percentage in each zone, as illustrated in Table 6. The dynamic percentage is selected in such a way that it is uniform within the zone, and any further increment may lead to voltage delay followed by transient instability. With this condition, the voltage recovery
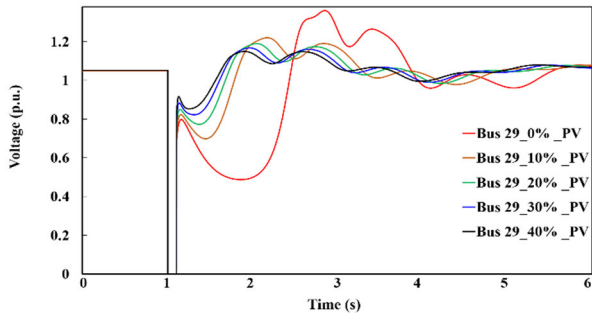
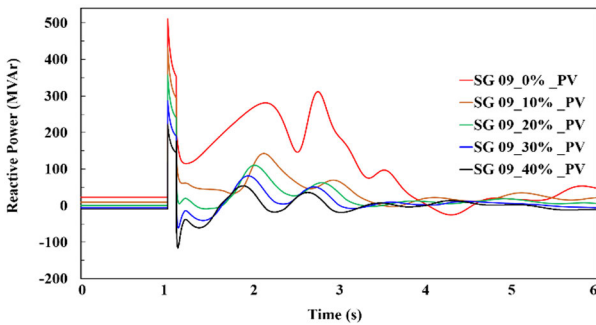**FIGURE 15.** Voltage profile under different PV levels – bus 29.

FIGURE 16. SG 9 reactive power profile under different PV levels.

FIGURE 18. Sub- transient performance of SG 9 & LSPV 9 with 10% PV: (a) voltage profile of bus 29, SG 9 & PV 9; (b) SG 9 reactive power; (c) SG 9 & PV 9 fault current; (d) LSPV 9 reactive power.

FIGURE 19. Sub- transient performance of SG 9 & LSPV 9 with 40% PV: (a) voltage profile of bus 29, SG 9 & PV 9; (b) SG 9 reactive power; (c) SG 9 & PV 9 fault current; (d) LSPV 9 reactive power.

is reduced and reach closer to the instability limit as given in Table 6.

From the prior section, it is evident that Zone 1, especially bus 29, is significantly affected by PV integration. Thus, the transient response of bus 29 is considered in details to identify the PV dynamic voltage signature under disturbances. Fig. 15 shows the voltage profile under a three-phase SC fault. To understand the PV signature and nature of the contribution, the reactive power output in each scenario are recorded and given as in Figs. 16 and 17.
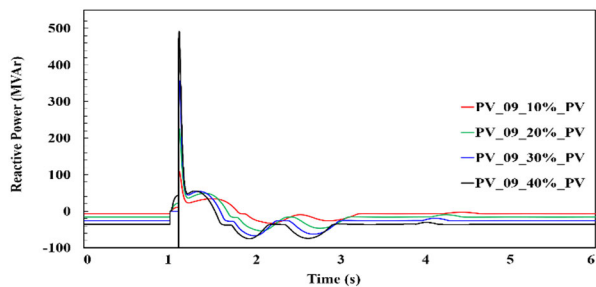
TABLE 7. The correlation coefficient between recovery indices.

	VRI	*VRT*	*QS-Transt*	*QTranst*
VRI	1.00	-0.73	0.16	-0.63
VRT	-	1.00	0.21	0.71
QS-Transt	-	-	1.00	0.39
QTranst	-	-	-	1.00

FIGURE 17. LSPV 9 reactive power profile under different PV levels.

The sub-transient contributions of SG 9 & LSPV 9 (the most influential generator of bus 29) are directly related to their MVA ratings. The transient contributions of SG & PV are governed by the transient performance of the load. Hence, the delayed voltage recovery may cause high demand for reactive current in the transient region. The inverter terminal voltage during the fault could reach to zero when the PV
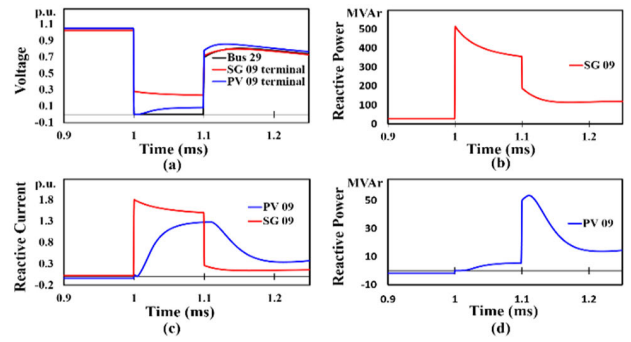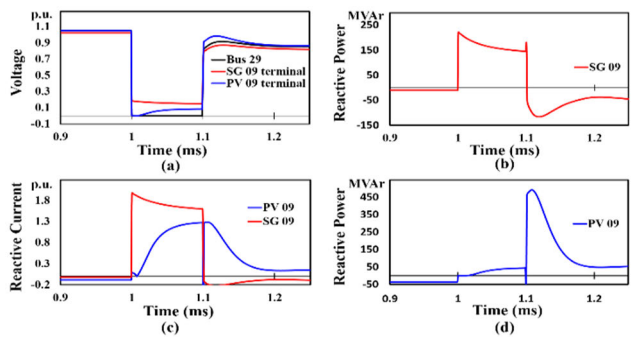
inverters operate in current control mode (grid following). Such a situation may block the grid following inverter from injecting reactive current during the first few cycles in the sub-transient region, as illustrated in Figs. 18 and 19. Moreover, it can be noticed that there is a delay in the response of the inverter during the sub-transient region. The response of this delay is similar to the capacitor response in charging and discharging.

The SG sub-transient response is harmonious with fault duration for all PV penetration levels. However, there could be a delay in the PV inverter sub-transient response. This delay results in injecting reactive power in the early stages of the transient region. Therefore, this response accelerates the voltage recovery and improves the voltage recovery time (*VRT*), as depicted in Fig. 20. For instance, the *VRT* of bus 29 is significantly improved from 74 cycles (1.23 seconds [60Hz system]) in the base case to 14 cycles (0.23 seconds)

TABLE 8. Voltage Recovery Index (VRI) variation for 40% PV.

| Bus #		03	04	07	08	15	16	18	21	23	24	25	26	27	28	29
								Fault Location								
%	03	-0.1	-0.5	-2.1	-2.1	1.1	9.0	0.3	3.3	5.0	3.9	4.0	10.1	2.4	9.9	132.2
	04	0.8	1.0	-0.6	-0.6	2.1	10.2	1.0	4.1	5.9	4.7	4.3	9.1	2.2	7.8	111.6
	07	1.3	1.9	0.3	0.3	2.5	10.5	1.3	4.3	6.1	5.0	4.6	8.9	2.3	7.3	105.7
	08	1.2	1.8	0.2	0.2	2.4	10.5	1.2	4.3	6.1	5.0	4.6	9.0	2.3	7.5	108.0
	15	0.4	-0.1	-2.3	-2.3	2.3	11.4	1.0	4.8	6.7	5.6	3.8	8.6	2.0	7.1	100.6
	16	0.3	-0.5	-2.9	-2.9	2.4	11.8	1.1	5.2	7.0	5.9	3.7	8.5	2.0	6.9	95.5
	18	0.1	-0.6	-2.7	-2.6	1.5	10.1	0.6	3.9	5.6	4.6	4.3	10.8	2.6	10.4	136.3
	21	0.2	-0.7	-3.2	-3.2	2.6	12.3	1.1	5.8	7.9	6.4	3.2	7.2	1.6	5.2	77.5
	23	0.2	-0.8	-3.3	-3.2	2.7	12.0	1.1	6.0	8.0	6.4	2.8	5.8	1.2	3.4	54.0
	24	0.3	-0.6	-3.0	-3.0	2.4	11.8	1.1	5.3	7.2	6.0	3.5	8.0	1.8	6.3	88.3
	25	0.3	-0.4	-1.9	-1.9	0.9	8.9	0.6	2.9	4.3	3.6	5.2	12.3	3.2	12.5	160.5
	26	1.3	-1.1	-3.6	-3.5	1.2	10.9	1.9	3.0	4.2	4.4	8.7	22.5	7.5	25.4	246.8
	27	0.8	-1.0	-3.4	-3.3	1.4	10.8	1.4	3.5	5.0	4.6	6.8	17.6	5.3	19.2	206.4
	28	4.0	-0.6	-4.2	-4.1	2.1	14.9	4.7	3.4	3.8	5.9	15.4	36.2	14.6	41.0	360.2
	29	5.0	-0.2	-4.0	-3.9	2.7	16.4	5.7	3.7	3.9	6.6	17.6	40.2	16.7	45.4	394.6

Voltage Recovery Index (VRI) Variation
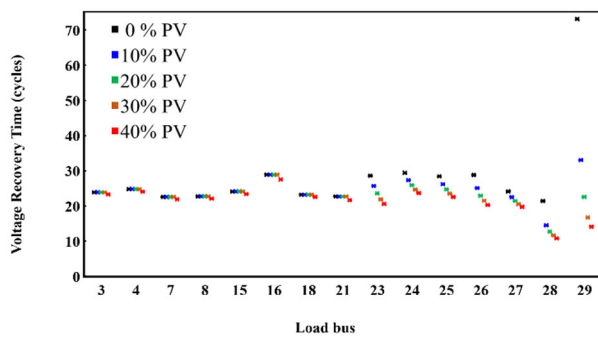
FIGURE 20. Load bus voltage recovery time.

with 40% PV penetration. The improvement in bus 29 VRT is corresponding to the huge amount of reactive power injected during the first few cycles of transient time as in Fig. 19 (c) & (d). Other buses in Zones 1 & 3 have experienced a better *VRT* with more PV penetration. Nevertheless, there is a minor change in the *VRT* of loads in Zone 2 when more PVs are connected to the network.

To explore the influence of LSPV integration on system dynamic performance, the VAr injected from SG and PV during the first few seconds after clearance of the fault is determined. The amount of *QS-Transt* and *QTranst* is used to understand the influence of PV. Table 7 shows the correlation coefficient between the VRI, VRT, *QS-Transt*, and *QTranst*. It can be seen that the voltage recovery is inversely correlated with the recovery time. VRI and VRT inverse correlation indicates that shorter VRT (faster recovery) should result in better transient response and a larger value of VRI. Moreover, the *QTranst* is inversely correlated with VRI (correlation coefficient R = −0.63). On the other hand, the VRI is poorly correlated with the VAr injected during the sub-transient region (R= 0.16). The *QTranst* is also highly correlated with

VRT, which indicates that a faster recovery results in lower demand for VAr during the transient region.

The system dynamic voltage signature has been explored when the fault happens at the PCC. It is found that PV could enhance system stability by improving the voltage recovery. However, as the SGs may have an area of influence in the interconnected network. The SGs retirement would significantly impact overall system strength, and load bus voltage recovery could be negatively influenced. Table 8 displays the impact of retiring 40% of SG 3 - 9 and replaces them with LSPV power plants. For a fault at any load bus in Zone 1 or Zone 3, the system may experience better performance. However, the system performance is slightly affected by the fault at buses 4, 7, and 8. In such a case, the impact of faults in Zone 2 could be seen at the Zone 1 buses. For example, if a fault happens at buses 7 or 8, the VRI of bus 26-29 would be reduced by 4%.

This research was not aimed to explore the optimal penetration level neither for renewable resources in general nor of the LSPV power plant in specific. However, the PV penetration level was chosen to be up to 40% achievable in several countries' foreseeable future. Therefore, the system response and dynamic voltage signature beyond 40% PV we're not considered. Moreover, it would not be easy to generalize the system voltage signature based on the current investigation outcomes by considering the power system complexity. In future work, the authors will explore dynamic system signature under a wider range of PV power plant penetration levels and including an energy storage system and other plant-level VAr support devices.

V. CONCLUSION

A framework for assessing the dynamic voltage signature with LSPV is presented in this article. A comprehensive steady-state and transient analyses has been considered to

comprehend the dynamic voltage signature of power system with LSPV plants. The research also aims at establishing connections between steady-state and transient in the context of voltage stability. In this work, the following issues are considered with respect to previous works:

- Consideration of the synchronous generator area of influence.
- Incorporation of inherent dynamic characteristics of synchronous generator parameters and the change of network topology.
- Deliberation of variability in load modelling and parameters including the penetration of LSPV.

From the results, it is evident that system topology and availability of number of synchronous generators may govern the dynamic voltage signature of the system. It is worth noting that there is no clear relationship between the short-circuit ratio-based raking and voltage recovery ranking of the buses to identify the focal point for system remedy. However, dynamic loads have a profound impact on dynamic voltage signature, and penetration of LSPV seems to favor hosting higher capacity of dynamic loads from dynamic voltage stability point of view.

This work only considered the aggregated load model at the transmission and sub-transmission voltage level. The influence of distribution level DER and load on the dynamic voltage signature of the system will be explored in the future. An online dynamic voltage signature identification will also be proposed in the future.

REFERENCES

[1] A. S. Bose and S. Sarkar, "India's e-reverse auctions (2017–2018) for allocating renewable energy capacity: An evaluation," *Renew. Sustain. Energy Rev.*, vol. 112, pp. 762–774, Sep. 2019.

[2] A. F. Almarshoud and E. Adam, "Towards VLS-PV deployment in Saudi Arabia: Challenges, opportunities and recommendations," *Energy Policy*, vol. 114, pp. 422–430, Mar. 2018.

[3] R. Shah, N. Mithulananthan, R. C. Bansal, and V. K. Ramachandaramurthy, "A review of key power system stability challenges for large-scale PV integration," *Renew. Sustain. Energy Rev.*, vol. 41, pp. 1423–1436, Jan. 2015.

[4] L. Meegahapola and T. Littler, "Characterisation of large disturbance rotor angle and voltage stability in interconnected power networks with distributed wind generation," *IET Renew. Power Gener.*, vol. 9, no. 3, pp. 272–283, Apr. 2015.

[5] K. W. Jones, P. Pourbeik, G. Kobet, A. Berner, N. Fischer, F. Huang, J. Holbach, M. Jensen, J. O'Connor, M. Patel, M. Ropp, J. Wen, T. Yang, R. D. Bauer, R. W. Cummings, R. D. Quint, N. Segal, M. Osman, and Task Force on Short-Circuit and System Performance Impact of Inverter Based Generation, "Impact of inverter based generation on bulk power system dynamics and short-circuit performance," IEEE Power Energy Soc., Tech. Rep. PESTR68, Jul. 2018, pp. 1–63.

[6] A. Cabrera-Tobar, E. Bullich-Massagué, M. Aragüés-Peñalba, and O. Gomis-Bellmunt, "Review of advanced grid requirements for the integration of large scale photovoltaic power plants in the transmission system," *Renew. Sustain. Energy Rev.*, vol. 62, pp. 971–987, Sep. 2016.

[7] T. Aziz, T. K. Saha, and N. Mithulananthan, "A review of interconnection rules for large-scale renewable power generation," in *Large Scale Renewable Power Generation*. Singapore: Springer, 2014, pp. 151–171.

[8] L. Meegahapola, M. Datta, I. Nutkani, and J. Conroy, "Role of fault ride-through strategies for power grids with 100% power electronic-interfaced distributed renewable energy resources," *Wiley Interdiscipl. Rev., Energy Environ.*, vol. 7, no. 4, p. e292, Jul. 2018.

[9] M. N. I. Sarkar, L. G. Meegahapola, and M. Datta, "Reactive power management in renewable rich power grids: A review of grid-codes, renewable generators, support devices, control strategies and optimization algorithms," *IEEE Access*, vol. 6, pp. 41458–41489, 2018.

[10] W. Qi, Z. Jian, L. Liping, L. Baiqing, L. Mingsong, L. Weifang, and S. Yao, "A dynamic reactive power reserve optimization method to enhance transient voltage stability," in *Proc. IEEE Int. Conf. Cyber Technol. Autom., Control, Intell. Syst. (CYBER)*, Jun. 2015, pp. 1523–1528.

[11] Z. H. Rather, Z. Chen, P. Thogersen, and P. Lund, "Dynamic reactive power compensation of large-scale wind integrated power system," *IEEE Trans. Power Syst.*, vol. 30, no. 5, pp. 2516–2526, Sep. 2015.

[12] A. Tiwari and V. Ajjarapu, "Optimal allocation of dynamic VAR support using mixed integer dynamic optimization," *IEEE Trans. Power Syst.*, vol. 26, no. 1, pp. 305–314, Feb. 2011.

[13] M. Paramasivam, A. Salloum, V. Ajjarapu, V. Vittal, N. B. Bhatt, and S. Liu, "Dynamic optimization based reactive power planning to mitigate slow voltage recovery and short term voltage instability," *IEEE Trans. Power Syst.*, vol. 28, no. 4, pp. 3865–3873, Nov. 2013.

[14] G. Lammert, *Modelling, Control and Stability Analysis of Photovoltaic Systems in Power System Dynamic Studies*. Kassel, Germany: Kassel Univ. Press GmbH, Jun. 2019.

[15] R. K. Varma and S. Mohan, "Mitigation of fault induced delayed voltage recovery (FIDVR) by PV-STATCOM," *IEEE Trans. Power Syst.*, vol. 35, no. 6, pp. 4251–4262, Nov. 2020.

[16] K. Kawabe and K. Tanaka, "Analytical method for short-term voltage stability using the stability boundary in the P-V plane," *IEEE Trans. Power Syst.*, vol. 29, no. 6, pp. 3041–3047, Nov. 2014.

[17] K. Kawabe, Y. Ota, A. Yokoyama, and K. Tanaka, "Novel dynamic voltage support capability of photovoltaic systems for improvement of short-term voltage stability in power systems," *IEEE Trans. Power Syst.*, vol. 32, no. 3, pp. 1796–1804, May 2017.

[18] R. Shah and N. Mithulananthan, "Test systems for dynamic stability studies in electric power system," in *Proc. Australas. Universities Power Eng. Conf. (AUPEC)*, Sep. 2013, pp. 1–6.

[19] R. Liu, J. Yao, X. Wang, P. Sun, J. Pei, and J. Hu, "Dynamic stability analysis and improved LVRT schemes of DFIG-based wind turbines during a symmetrical fault in a weak grid," *IEEE Trans. Power Electron.*, vol. 35, no. 1, pp. 303–318, Jan. 2020.

[20] *The 39 Bus New England System*, DIgSILENT, GmbH, Heinrich-Hertz-Str., Germany, 2019.

[21] *WECC Solar Plant Dynamic Modeling Guidelines*, WECC Renew. Energy Model. Task Force, Salt Lake City, UT, USA, 2014.

[22] *National Electricity Rules_Version 126*, Austral. Energy Market Commission (AEMC), Sydney, NSW, Australia, Nov. 2019.

[23] A. Q. Al-Shetwi, M. A. Hannan, K. P. Jern, M. Mansur, and T. M. I. Mahlia, "Grid-connected renewable energy sources: Review of the recent integration requirements and control methods," *J. Cleaner Prod.*, vol. 253, Apr. 2020, Art. no. 119831.

[24] L. Kong, G. Cai, S. Xue, and S. Li, "Modeling and coordinated control strategy of large scale grid-connected wind/photovoltaic/energy storage hybrid energy conversion system," *Math. Problems Eng.*, vol. 2015, pp. 1–14, Jan. 2015.

[25] S. Alzahrani, R. Shah, N. Mithulananthan, and A. Sode-Yome, "Large-scale PV voltage regulation: Survey of recent practice," in *Proc. IEEE PES GTD Grand Int. Conf. Expo. Asia (GTD Asia)*, Mar. 2019, pp. 661–666.

[26] J. V. Milanovic, K. Yamashita, S. Martinez Villanueva, S. Z. Djokic, and L. M. Korunovic, "International industry practice on power system load modeling," *IEEE Trans. Power Syst.*, vol. 28, no. 3, pp. 3038–3046, Aug. 2013.

[27] J. Milanovic, J. Matevosyan, A. Gaikwad, A. Borghetti, S. Djokic, Z. Dong, H. Andrew, L. Korunovic, S. M. Villanueva, J. Ma, P. Pourbeik, F. Resende, S. Sterpu, F. Villella, K. Yamashita, O. Auer, K. Karoui, D. Kosterev, and Y. Xu, "Modelling and aggregation of loads in flexible power networks," CIGRE, Paris, France, Tech. Rep. WG C4.605, Feb. 2014, pp. 1–191.

[28] Y. Zhu, "Ranking of power system loads based on their influence on power system stability," M.S. thesis, School Elect. Electron. Eng., Univ. Manchester, Manchester, U.K., 2019. [Online]. Available: https://www.escholar.manchester.ac.uk/uk-ac-man-scw:319348

[29] Y. Zhu, J. V. Milanović, and K. N. Hasan, "Ranking and quantifying the effects of load model parameters on power system stability," *IET Gener., Transmiss. Distrib.*, vol. 13, no. 20, pp. 4650–4658, Oct. 2019.

[30] H. Saadat, *Power System Analysis*. New York, NY, USA: McGraw-Hill, 1999, pp. 314–352.

[31] E. Munkhchuluun, L. Meegahapola, and A. Vahidnia, "Impact on rotor angle stability with high solar-PV generation in power networks," in *Proc. IEEE PES Innov. Smart Grid Technol. Conf. Eur. (ISGT-Europe)*, Sep. 2017, pp. 1–6.

[32] K. Kawabe and T. Nanahara, "Integration of dynamic voltage support capability of distributed photovoltaic generation systems for transient stability improvement of power systems," in *Proc. IEEE PES Innov. Smart Grid Technol. Conf. Eur. (ISGT-Europe)*, Oct. 2018, pp. 1–6.

RAKIBUZZAMAN SHAH (Member, IEEE) is currently a Senior Lecturer in smart power systems engineering with the School of Engineering, Information Technology and Physical Sciences, Federation University Australia (FedUni Australia). Before joining FedUni Australia, he has worked with The University of Manchester, The University of Queensland, and Central Queensland University. He has experience working at, and consulting with, DNOs and TSOs on individual projects and collaborative work on a large number of projects (EPSRC project on Multi-terminal HVDC, Scottish, and Southern Energy Multi-infeed HVDC)—primarily on the dynamic impact of integrating new technologies and power electronics into large systems. He has more than 70 international publications (journals and conferences) and has spoken at the leading power system conferences around the world. His research interests include future power grids (i.e., renewable energy integration and wide-area control), asynchronous grid connection through VSC-HVDC, power system stability and dynamics, application of data mining in power systems, application of control theory in power systems, distribution system energy management, and low-carbon energy systems.

NADARAJAH MITHULANANTHAN (Senior Member, IEEE) received the B.Sc. (Eng.) degree from the University of Peradeniya, Sri Lanka, the M.Eng. degree from the Asian Institute of Technology (AIT), Bangkok, and the Ph.D. degree from the University of Waterloo, ON, Canada.

Prior to joining The University of Queensland, he was attached to Energy Field of Study at AIT. His previous professional positions include a Planning Engineer at the Generation Planning Division, Ceylon Electricity Board, Sri Lanka, for two years, and the Project Leader at the Centre of Excellence in Electric Power Technology, Chulalongkorn University, Thailand, for one year. He has been the Director of higher degree research training and a Post Graduate Coordinator with the School of Information Technology and Electrical Engineering, The University of Queensland, since July 2019. His main research interests include analytical studies on electric power grids, power system stability and dynamics, grid integration of renewable energy, battery energy storage, and electric vehicle charging stations.

SAEED ALZAHRANI (Student Member, IEEE) received the B.Sc. degree in engineering from the King Fahd University of Petroleum and Minerals (KFUPM), Saudi Arabia, in 2009, and the M.Eng. degree from The University of Queensland, Brisbane, Australia, in 2015, where he is currently pursuing the Ph.D. degree with the Power, Energy and Control Engineering Research Group, School of Information Technology and Electrical Engineering. His main research interests include large-scale renewable energy integration and power system stability studies.

• • •